

## Article

# Development of Backfill Concrete Including Coal Gangue and Metakaolin and Prediction of Compressive Strength by Extreme Learning Machine

Jiaxu Jin <sup>1,2</sup>, Shihao Yuan <sup>1,\*</sup>, Zhiqiang Lv <sup>1,\*</sup> and Qi Sun <sup>1</sup>

<sup>1</sup> Department of Civil Engineering, Liaoning Technical University, Fuxin 123000, China; jinjiaxu@lntu.edu.cn (J.J.); 471920428@stu.lntu.edu.cn (Q.S.)

<sup>2</sup> Liaoning Key Laboratory of Mine Subsidence Disaster Prevention and Control, Liaoning Technical University, Fuxin 123000, China

\* Correspondence: 471920510@stu.lntu.edu.cn (S.Y.); 472020626@stu.lntu.edu.cn (Z.L.)

**Abstract:** The main aim of this investigation is to develop backfill concrete including coal gangue and metakaolin to reduce solid waste. For this purpose, a total of 30 concrete mixtures were designed by the inclusion of 0%, 25%, 50%, 75% and 100% coal gangue as coarse aggregates and 0%, 10% and 20% metakaolin as binder at 0.55 and 0.45 water to cement ratios. The compressive strength was tested after 3, 7 and 28 days for a total of 90 samples. Meanwhile, the influences of coal gangue and metakaolin on the elastic modulus, ultrasonic pulse velocity, rebound number and open porosity were explored. Then, the relationship between physical and mechanical properties was revealed by design code expressions and empirical models. Furthermore, an extreme learning machine was developed to predict compressive strength by concrete mixtures. The results show that the inclusion of coal gangue results in a poor performance in physical and mechanical properties of concrete. However, the drawbacks of concrete containing coal gangue can be compensated by metakaolin. The predicted results of design code expressions and empirical models are closed to the experiment results, with a 10% error. In addition, the findings reveal that the extreme learning machine offers significant potential to predict the compressive strength of concrete with high precision.

**Keywords:** backfill concrete; coal gangue; metakaolin; extreme learning machine; physical and mechanical properties



**Citation:** Jin, J.; Yuan, S.; Lv, Z.; Sun, Q. Development of Backfill Concrete Including Coal Gangue and Metakaolin and Prediction of Compressive Strength by Extreme Learning Machine. *Minerals* **2022**, *12*, 330. <https://doi.org/10.3390/min12030330>

Academic Editors: Yanli Huang, Junmeng Li and Carlito Tabelin

Received: 23 January 2022

Accepted: 3 March 2022

Published: 7 March 2022

**Publisher's Note:** MDPI stays neutral with regard to jurisdictional claims in published maps and institutional affiliations.



**Copyright:** © 2022 by the authors. Licensee MDPI, Basel, Switzerland. This article is an open access article distributed under the terms and conditions of the Creative Commons Attribution (CC BY) license (<https://creativecommons.org/licenses/by/4.0/>).

## 1. Introduction

The rapid development of infrastructure has seen a dramatic increase in the consumption of construction materials [1]. Concrete, as a composite material, plays a key role in industrial, civil and military constructions [2]. The demand for concrete is estimated to increase to nearly 16 billion tones [3]. Aggregate is the most important component of concrete, accounting for more than 70% of the volume [4,5]. Coarse aggregate acts as the skeleton and support of concrete. However, the exploitation of natural coarse aggregates (i.e., crushed stone, gravel) has resulted in an imbalance of resources and the environment in certain regions, especially in Bangladesh, China and India [6]. Therefore, it is urgent to find alternative coarse aggregates [7].

Considerable amounts of solid wastes are favorable candidates for coarse aggregate. Repurposing mining wastes reduces the final volume that ends up in tailings storage facilities, which is beneficial to mining operations and the environment [8–14]. The utilization of mining waste in cemented backfill, such as tailings and coal gangues (CG), is of great benefit for the eco-environment and can control the Earth's surface subsidence well. Among them, coal cleaning tailings and rejects, produced from coal mining as industrial residue, is tantamount to about 10–15% of the total mass of coal. In 2019, almost 4.5 billion tons of CG was discharged in China. Waste CG occupies tremendous land and is also harmful

to the environment [15–17]. A similar scenario is encountered in other countries [18,19]. Therefore, finding an appropriate approach to make full use of CG has become a matter of urgency. There are two predominant applications for CG: power generation and building materials [20]. In fact, the application of CG as a coarse aggregate in concrete is a simple and feasible method [20]. Currently, more recent attention has focused on the provision of CG as a substitute for coarse aggregate. Surveys such as that conducted by Li (2021) have shown that the fluidity loss of fresh concrete was due to the porous structure of CG with high water absorption capacity [4]. Data from several sources have identified the decreased mechanical properties associated with the inclusion of CG in concrete [21,22]. The results documented that a significant decrease was found in the compressive and flexural strength of concrete. Furthermore, the loss of mechanical properties is more than 20% in concrete where CG completely replaces coarse aggregate [2]. In addition to the mechanical properties, poor performance has been shown in the shrinkage and durability of concrete containing CG [10].

The studies presented thus far provide evidence that CG replacing coarse aggregate leads to the degradation in concrete properties. This is the main reason that CG has not been widely used in the production of concrete. So far, only fly ash incorporation has been attempted to compensate the degradation properties of concrete containing 40% CG substitution [21]. As reported in previous studies, the usage of geopolymers is practical to improve the quality of concrete [23–26]. Metakaolin, as a geopolymer, is extensively applied as a reinforcement of concrete. Traditionally, it has been argued that metakaolin is beneficial for the improvement in the physical and mechanical properties of concrete. It has been revealed that metakaolin can improve the water absorption and permeability of concrete [27–29]. In addition, metakaolin was found to be responsible for the enhanced mechanical properties of concretes [30,31]. Furthermore, it is also observed that the use of metakaolin can compensate for the loss of recycled concrete's strength to the level of conventional concrete [32–34]. These studies evidenced that the applicability of metakaolin has an encouraging impact on concrete. However, far too little attention has been paid to the use of metakaolin in concrete containing CG.

The main purpose of this study is to develop an understanding on the development of physical and mechanical properties of concrete containing both CG and metakaolin. First, the influences of CG and metakaolin on the compressive strength, elastic modulus, ultrasonic pulse velocity, rebound number and open porosity of concrete were conducted. Then, a comparative analysis was explored on experimental, code expressions and empirical model results. Finally, a powerful analytical method, an extreme learning machine (ELM), is proposed to predict the compressive strength of concrete.

## 2. Experimental Programs

### 2.1. Materials

Ordinary Portland cement (OPC) of P·O 42.5 complied with GB175-2007 and ground metakaolin were employed as binders [35]. The physical index and chemical composition of OPC and metakaolin are listed in Table 1. The fine metakaolin particles led to the filler effect. High surface area of  $\text{SiO}_2$  and  $\text{Al}_2\text{O}_3$  contributed to accelerated hydration and pozzolanic reaction. Natural river sand with fineness modulus of 2.65 was selected for fine aggregate, with an apparent density of  $2860 \text{ kg/m}^3$ . CG was attained from a coal mine in Fuxin. According to national regulations, the size of the specimen is more than three times the maximum particle size. After sieving, CGs with a continuous grading ranging from 5 to 25 mm were employed. The details of CG have been reported in [36]. Among them, the material properties, manufacturing processes and strength grades selected in this paper are all different. The water absorption, crushing index and apparent densities were 5.7%, 18.9% and  $2.35 \text{ g/cm}^3$ , respectively. Beyond that, the biggest challenge in reusing mining waste is its potential to release harmful elements into the environment. The CG samples were previously considered harmless [37,38].

**Table 1.** The physical index and chemical composition of OPC and metakaolin.

Chemicals (wt %)	Physical Index			Chemical Composition (wt %)						
	Specific Surface Area (m <sup>2</sup> /g)	Density (g/cm <sup>3</sup> )	Average Diameter (μm)	SiO <sub>2</sub>	Al <sub>2</sub> O <sub>3</sub>	Fe <sub>2</sub> O <sub>3</sub>	MgO	CaO	LOI	Total
OPC	0.36	3.18	24	22.45	5.4	4.7	1.7	61.75	2.37	98.37
Metakaolin	33.60	2.67	0.57	53.43	42.5	1.28	0.36	0.24	1.10	98.91
CG	-	2.35	-	63.52	19.31	0.93	0.71	2.31	6.45	93.23

### 2.2. Concrete Mixes and Samples Preparation

A total of 30 mixtures were designed to explore the physical and mechanical properties of concrete with metakaolin and CG, and 3 samples of each mixture were tested. The concrete was prepared with 0%, 25%, 50%, 75% and 100% CG replacement. For each of the above mixtures, three metakaolin percentage levels (i.e., 0%, 10%, 20%) were designed. Moreover, two water–cement ( $w/c$ ) ratios (i.e., 0.45, 0.55) were applied for each mixture. The details of each mixture are given in Table 2. Prior to the experiment, prewetting was performed on CG given its porous structure. Then, a uniform solid mixture was prepared consisting of cementitious material and fine and coarse aggregates. The water was then added to prepare a uniform slurry by stirring. Lastly, the fully mixture was cast in mold with a size of 100 mm × 100 mm × 100 mm and demolded after 24 h. The samples were cured at a standard curing condition (20 ± 2 °C, 98% RH) until the specified ages (3 days, 7 days, 28 days).

**Table 2.** The mix proportions of the concrete samples.

$w/c$	Sample	Water (kg/m <sup>3</sup> )	OPC (kg/m <sup>3</sup> )	Metakaolin (kg/m <sup>3</sup> )	Sand (kg/m <sup>3</sup> )	Gravel (kg/m <sup>3</sup> )	CG (kg/m <sup>3</sup> )
0.55	CG0MK0	210	382	0	650	1020	0
	CG0MK10	210	343.8	38.2	650	1020	0
	CG0MK20	210	305.6	76.4	650	1020	0
	CG25MK0	210	382	0	650	765	255
	CG25MK10	210	343.8	38.2	650	765	255
	CG25MK20	210	305.6	76.4	650	765	255
	CG50MK0	210	382	0	650	510	510
	CG50MK10	210	343.8	38.2	650	510	510
	CG50MK20	210	305.6	76.4	650	510	510
	CG75MK0	210	382	0	650	255	765
	CG75MK10	210	343.8	38.2	650	255	765
	CG75MK20	210	305.6	76.4	650	255	765
	CG100MK0	210	382	0	650	0	1020
	CG100MK10	210	343.8	38.2	650	0	1020
	CG100MK20	210	305.6	76.4	650	0	1020
0.45	CG0MK0	185	411	0	682	1218	0
	CG0MK10	185	369.9	41.1	682	1218	0
	CG0MK20	185	328.8	82.2	682	1218	0
	CG25MK0	185	411	0	682	913.5	304.5
	CG25MK10	185	369.9	41.1	682	913.5	304.5
	CG25MK20	185	328.8	82.2	682	913.5	304.5
	CG50MK0	185	411	0	682	609	609
	CG50MK10	185	369.9	41.1	682	609	609
	CG50MK20	185	328.8	82.2	682	609	609
	CG75MK0	185	411	0	682	304.5	913.5
	CG75MK10	185	369.9	41.1	682	304.5	913.5
	CG75MK20	185	328.8	82.2	682	304.5	913.5
	CG100MK0	185	411	0	682	0	1218
	CG100MK10	185	369.9	41.1	682	0	1218
	CG100MK20	185	328.8	82.2	682	0	1218

### 2.3. Testing of Specimens

The compressive strength of the specified age sample was performed by 2000kN servo test system. Meanwhile, the deformation was recorded by DH 3818 acquisition instrument. The compressive strength and elastic modulus were calculated according to

the code of GB/T 50081-2019 [39]. The GTJ-U820 ultrasonic instrument was employed to determine Ultrasonic pulse velocity based on CECS 21:2000 [40]. Rebound number was determined from 16 measuring points using GTJ-HT225B rebound instrument complied with the guidelines of JGJ/T 23-2011 [41]. Open porosity was conducted according to ASTM C642 (2013) [42].

### 3. Results and Discussion

#### 3.1. Compressive Strength

The compressive strength of concrete is the most critical index of its design and performance. Figure 1 shows the compressive strength of concrete with CG and metakaolin with curing ages of 3, 7 and 28 days and  $w/c$  ratios of 0.55 and 0.45. It can be noticed that there is a steady drop in the compressive strength of the sample with the increase in CG addition regardless of curing ages and  $w/c$  ratios. With a  $w/c$  ratio of 0.55, the 3 day compressive strengths of the samples (without metakaolin) containing 25%, 50%, 75% and 100% CG were 17.95 MPa, 17.38 MPa, 17.00 MPa and 16.31 MPa, respectively, presenting a 2.70%, 5.79%, 7.86% and 11.60% decline in compressive strength relative to the control sample (CG0MK0). The 7 day compressive strengths of the sample without metakaolin ranges from 23.20 MPa to 26.99 MPa. There is a 14.70% decrease in the 7 day compressive strength of concrete with 100% CG compared to the control sample. The 28 day compressive strengths also show a similar variation trend. The 28 day compressive strength of the control sample is 35.45 MPa, which declines to 33.77 MPa, 32.43 MPa, 30.72 MPa and 28.04 MPa for the samples containing 25%, 50%, 75% and 100% CG (CG25MK0, CG50MK0, CG75MK0 and CG100MK0), respectively indicating a 4.81%, 8.59%, 13.42% and 20.96% drop in compressive strength for the corresponding addition of CG. At the 0.45  $w/c$  ratio, a similar compressive strength degradation is found with the increase in CG, as shown in Figure 1b. The inclusion of 25%, 50%, 75% and 100% CG in concrete results in a 3.81%, 7.92%, 10.63% and 14.78% decrease in the 3 day compressive strength of concrete. The 7 day compressive strength of samples with 100% CG is reduced by 30.08% compared to that of the control sample (32.27 MPa). Similarly, it can be observed that the incorporation of 25%, 50%, 75% and 100% CG in samples reduces the 28 day compressive strength to 47.50 MPa, 41.83 MPa, 39.78 MPa and 38.17 MPa, respectively, which is 5.30%, 16.61%, 20.73% and 23.90 lower than that of the control sample, respectively.

It can be concluded that the incorporation of CG has an obvious negative effect on the compressive strength of concrete. To some extent, porous structures of CG absorb moisture from the mortar aggregate interface, reducing the  $w/c$  ratio and thus leading to finer and denser interfacial transition zone structures. However, it seems that this effect contributes little to concrete strength, whereas the relatively lower stiffness and elastic modulus of CG than those of gravel (coarse aggregate) may be the main reason for the decline in concrete strength. The stiffness and modulus of CG are derived from microscopic mechanical properties, which has been confirmed by Li [4]. Meanwhile, the highly porous microstructure of CG directly leads to stress concentration, which plays an important role in the strength of concrete. In general, there is an inverse relationship between the compressive strength of concrete and the content of CG. The results are in line with [43,44]. In addition, the degree of decline in the strength of concrete containing CG is also related to the  $w/c$  ratios and curing ages, as shown in Figure 1. Higher water cement ratios correspond to a milder strength deterioration. This may be due to the large amount of water absorbed by CG at the high  $w/c$  ratio. On the other hand, the degradation of strength increases with the curing age, which might be related to the low solidness and crushing value of CG.

Another result is that metakaolin improves the compressive strength of concrete, as shown in Figure 1. It can be found from Figure 1a that the addition of 10% metakaolin in sample (without CG) exhibits 16.73%, 13.54% and 17.36% enhancement in compressive strength as compared to control samples at 3 days, 7 days and 28 days, with a 0.55  $w/c$  ratio. In addition, the inclusion of metakaolin in the sample with a 0.45  $w/c$  ratio (CG0MK10) indicates 13.68%, 20.14% and 13.38% improvements in the 3-day, 7-day and 28-day compressive

sive strengths, respectively. In addition, it is noticed that the incorporation of metakaolin can mitigate the strength degradation of concrete with CG regardless of curing ages and the  $w/c$  ratio. At the 10% percentage replacement level and the 0.55  $w/c$  ratio, the 7-day compressive strengths of the samples are 21.53 MPa, 20.01 MPa, 13.06 MPa, 17.95 MPa and 17.14 MPa for 0%, 25%, 50%, 75% and 100% coarse aggregate replacement levels (CG0MK10, CG25MK10, CG50MK10, CG75MK10 and CG100MK10), respectively, which are 16.71%, 11.47%, 5.60% and 5.09% higher than that of the corresponding samples (with the same replacement level of coarse aggregate) without metakaolin. The 7-day compressive strengths of the samples containing 0%, 25%, 50%, 75% and 100% CG with 10% metakaolin increase by 13.7%, 7.42%, 9.49%, 6.50% and 7.06%, respectively. At the 28 day curing age, the improvement effect of metakaolin on the compressive strength of the samples is between 15% and 21%. The enhancement can be also found in concrete containing 20% metakaolin. However, the enhancement is weakened due to the dilution effect. Comparing Figure 1a,b, it can be easily deduced that metakaolin is also beneficial as the  $w/c$  ratio decreases from 0.55 to 0.45.

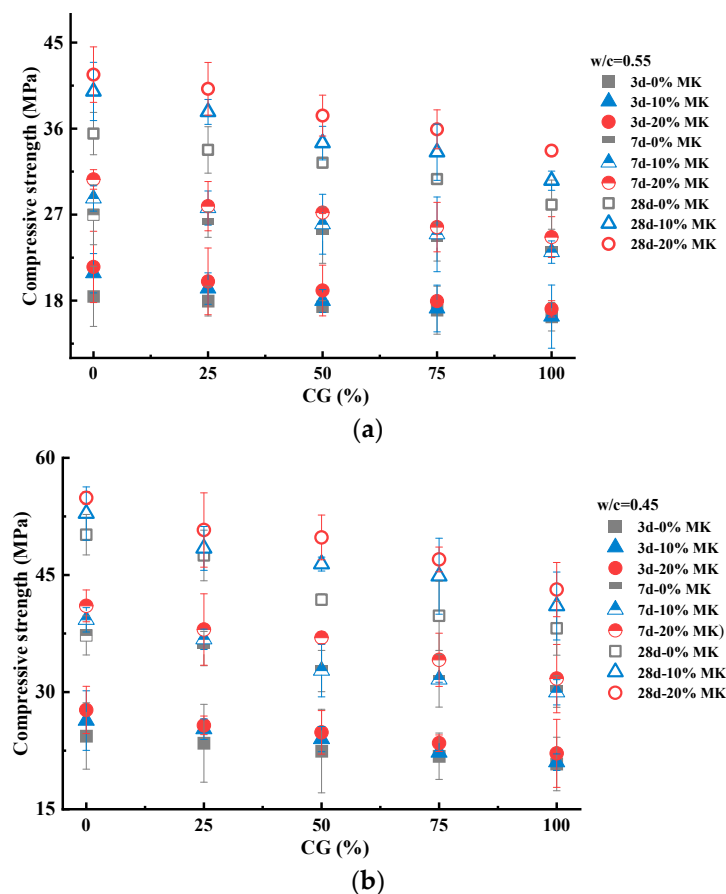


**Figure 1.** Variation of compressive strength of concrete with CG and metakaolin ((a) 0.55, (b) 0.45).

It can be found from Figure 1 that the addition of metakaolin has a positive effect on the compressive strength of concrete. There are both physical and chemical improvement mechanisms for metakaolin. The most important physical mechanism is the filler effect due to the fine particle size of metakaolin. According to the density theory, partial harmful pores in the structure of the concrete can be transformed into gel pores by adding appropriate fine metakaolin particles. Hua proved that gel pores were harmless in exploring the relationship between pores and compressive strength [45]. On the other hand, it is well-known that the pozzolanic reaction is representative of chemical improvement mechanisms. The reactive  $\text{SiO}_2$  in metakaolin can react with  $\text{Ca}(\text{OH})_2$  to produce additional hydrated calcium silicate (C-S-H) [46,47]. The C-S-H gels can not only have a filler effect, by forming

a more stable pore structure, but also have superior mechanical properties and chemical stability compared to  $\text{Ca}(\text{OH})_2$  [48]. However, there is a slight decrease in the strengthening effect on the compressive strength of concrete containing 20% metakaolin replacement level, which is associated with the dilution effect. Furthermore, the strengthening effect is affected by the  $w/c$  ratio. The improvement effect of metakaolin is more obvious in the samples with a high  $w/c$  ratio, which may be due to the greater defects in the samples with the 0.55  $w/c$  ratio.

### 3.2. Elastic Modulus

Figure 2 shows the effect of CG and metakaolin on elastic modulus of concrete. It can be seen that the elastic modulus of the samples with a  $w/c$  ratio of 0.55 ranges from 24.08 to 29.00GPa, with a variation range of 18.23%. The full substitution of CG for the coarse aggregate (CG100MK0) shows the lowest elastic modulus of 24.08GPa, which is a 10.67% decrease compared to the control sample. The highest elasticity modulus is found to be 29.00GPa in the specimens incorporating 10% metakaolin and 0% GG with a 0.55  $w/c$  ratio. Additionally, the elastic modulus ranges from 26.50GPa to 33.02GPa, and the variation range is about 24.59% for the sample with a  $w/c$  ratio of 0.45. Compared to the control sample, the elastic modulus of the sample with 100% CG decreases to 18.03%. In addition, only a 2.13% increase in the elastic modulus is found in the specimen without CG but with 10% metakaolin. Similar experimental results were proved in Dadsetan's work, where the incorporation of metakaolin showed a slight improvement in the elastic modulus [49]. However, the addition of CG results in a significant decrease in the elastic modulus, which is related to the low stiffness of CG. The result from Li has revealed that the stiffness of various components in CG is lower than that of gravel [4].

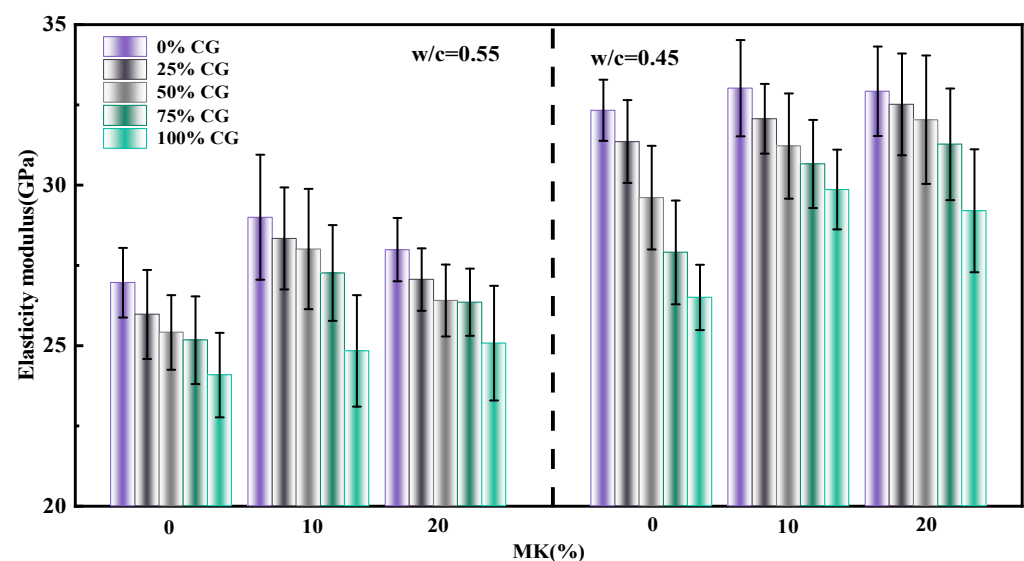


Figure 2. The elasticity modulus of the different concrete mixtures.

### 3.3. Ultrasonic Pulse Velocity

Figure 3 shows the variation of ultrasonic pulse velocity of concrete samples with different metakaolin and CG replacement levels. It can be clearly seen that metakaolin improves while the CG decreases the ultrasonic pulse velocity of sample. The ultrasonic pulse velocity displays a little fall for the sample with less than 50% CG, which sees a steep decline when the CG addition beyond 50%, however. At  $w/c$  ratio of 0.55, The ultrasonic pulse velocities are 3.07 km/s, 2.85 km/s, 2.73 km/s, 2.68 km/s and 2.44 km/s respectively for the control samples and the samples containing 25%, 50%, 75% and 100% CG (CG0MK0, CG25MK0, CG50MK0, CG75MK0, CG100MK0). The ultrasonic pulse velocity of control sample with a 0.45  $w/c$  ratio is 4.25km/s, and the corresponding declines in ultrasonic pulse velocity of concrete with 25%, 50%, 70% and 100% CG are found to be 5.73%, 11.01%,

18.19% and 26.38%, respectively. With a metakaolin replacement level of 10%, the samples containing 100% CG displayed a decrease of 17.77% and 16.90% compared with the samples without CG at  $w/c$  ratios of 0.55 and 0.45. Analogously, there are drops of 17.31% and 22.56% in the corporation of 20% metakaolin and 100% CG in samples with mixed up 0.55 and 0.45  $w/c$  ratios. Obviously, metakaolin results in an improvement in ultrasonic pulse velocity, which is consistent with Dabbaghi [30]. Whilst, the addition of CG in sample leads to the attenuation of ultrasonic pulse velocity, which is attributed to the porous structure of CG. As reported in ref [50], ultrasonic pulse velocity is an index reflecting the integrity of the internal structure of concrete materials. This means that the attenuation of ultrasonic wave velocity represents the more discrete microstructure of concrete due to the incorporation of CG.

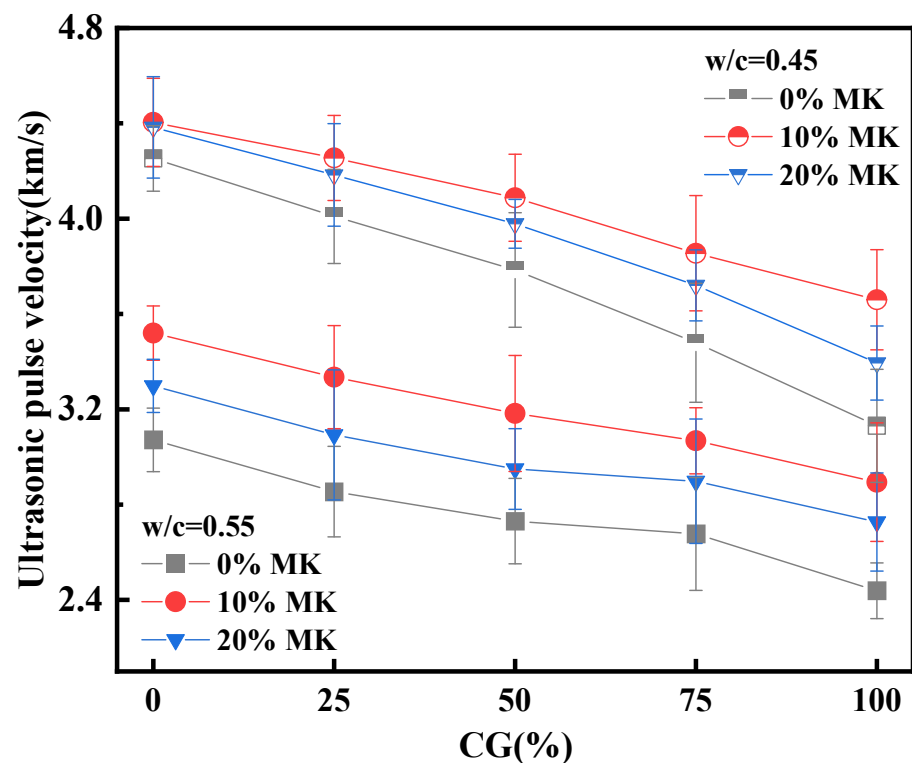


Figure 3. Variation of ultrasonic pulse velocity of different concrete mixtures.

### 3.4. Rebound Number

Figure 4 presents the rebound number of the sample after the addition of CG and metakaolin. It can be observed that the incorporation of 10% metakaolin achieved the most excellent performance in the rebound number of all specimens. At 0.55  $w/c$  ratio, the corporation of 10% metakaolin in samples containing 0%, 25%, 50%, 75% and 100% CG gain 14.23%, 19.96%, 15.92%, 17.87% and 13.30% increase in rebound number. Similarly, there is an increase between 4.12% and 7.83% corresponding to the incorporation of 10% metakaolin regardless of the replacement level of CG at a  $w/c$  ratio of 0.45. Meanwhile, a slight improvement in the rebound number was found due to the incorporation of 20% metakaolin. The improvement of the rebound number increased between 6.20% and 10.70% for samples containing 20% metakaolin at 0.55  $w/c$  ratio. It is also found that there is a 0.78–2.05% increase in rebound number for the samples containing 20% metakaolin at 0.45  $w/c$  ratio. As discussed above, metakaolin has an enhancement effect on concrete, especially for specimens with a  $w/c$  ratio of 0.55. This is due to the low homogeneity and high dispersion in concrete with higher  $w/c$  ratio.

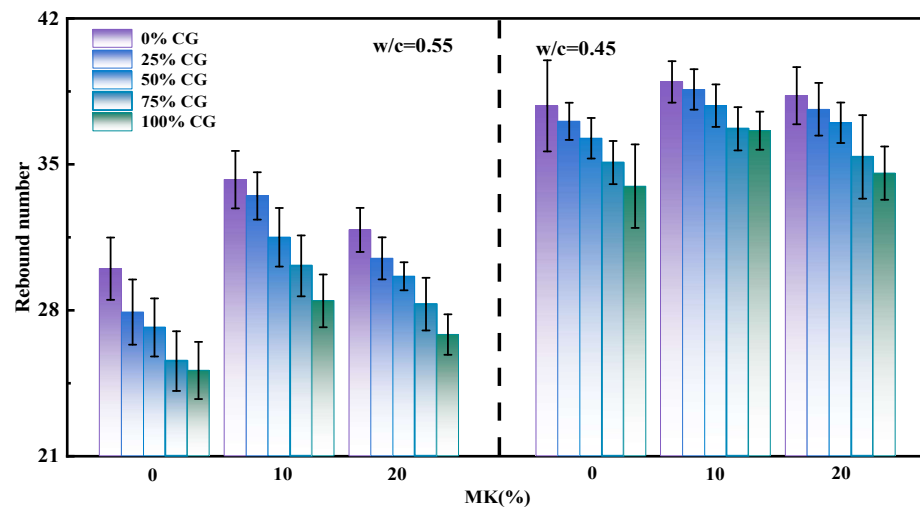


Figure 4. Variation of rebound number.

### 3.5. Open Porosity

The variation in the open porosity of the samples are tabulated in Table 3. It can be observed that there is a steady increase in the open porosity as the percentage of CG increases in the sample. At a 0.55  $w/c$  ratio, a fall in the open porosity values by 6.58%, 9.68%, 13.64% and 23.32% is noticed for the replacement level of coarse aggregate at 25%, 50%, 75% and 100% CG, respectively. a similar trend is found in samples with a 0.45  $w/c$  ratio. It can be observed that the open porosities of the samples incorporating 25%, 50%, 75% and 100% CG are 8.75%, 9.49%, 9.89% and 10.63%, respectively, which are 11.60%, 21.04%, 26.18% and 35.58% higher than that of the control sample. Open porosity is negatively correlated with density, cracks and uniformity. The presence of the porosity of CG increases the pore system in concrete. Unsurprisingly, the percentage of open porosity is significantly reduced due to the addition of metakaolin. However, the improvement in the open porosity increased first and then decreased as the percentage of metakaolin increased. The inclusion of 10% metakaolin achieves a superior performance in terms of open porosity. A drop in the open porosity values by 10.20% and 5.23% is realized for the control samples with 0.55 and 0.45  $w/c$  ratios, respectively. It is seen from the addition of 20% metakaolin in Table 3 that the open porosity is 7.04% and 7.43%, respectively, which represent a 9.18% and 5.23% reduction in the control specimen mixed with 0.55 and 0.45  $w/c$  ratios, respectively. This decline in open porosity is due to the filler effect by finer particles and pozzolanic reaction of metakaolin.

Table 3. Open porosity of the concrete specimens.

$w/c$	Sample	Open Porosity (%)				
		0% CG	25% CG	50% CG	75% CG	100% CG
0.55	0% MK	16.12	17.18	17.68	18.32	19.88
	10% MK	14.09	14.6	15.99	16.2	17.72
	20% MK	14.64	15.53	17.3	17.81	18.29
0.45	0% MK	7.84	8.75	9.49	9.89	10.63
	10% MK	7.04	7.7	8.25	8.79	9.53
	20% MK	7.43	7.94	8.82	9.21	10.42

### 3.6. SEM

The physical and mechanical properties depend on the microstructure of concrete. The addition of metakaolin results in the improvement in homogeneity of the microstructure. The samples with a 0.45  $w/c$  ratio were taken as examples to discuss the influence of metakaolin on the microstructure of concrete, as shown in Figure 5. Figure 5a shows the

microstructure of sample without metakaolin. It can be found that the main hydration products are fluffy C-S-H and plate-like  $\text{Ca}(\text{OH})_2$ . The main hydration products are C-S-H in specimens with 10% and 20% metakaolin, as shown in Figure 5b,c. As reported in [31], metakaolin can consume  $\text{Ca}(\text{OH})_2$  to produce additional C-S-H, which results in high compactness and uniformity. In addition, the inclusion of 20% metakaolin lead to cracks in concrete, due to high water absorption. This phenomenon may play a major role in the strength deterioration.

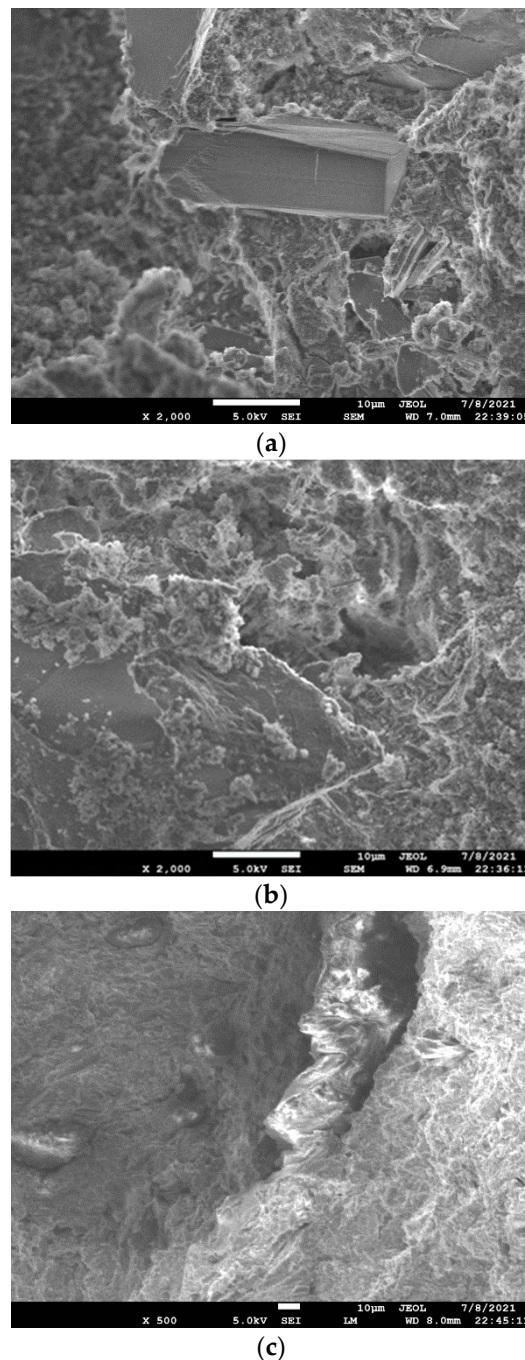


**Figure 5.** The microstructure of concrete at 0.45  $w/c$  ratio ((a) 0% metakaolin, (b) 10% metakaolin, (c) 20% metakaolin).

### 3.7. XRD

The microstructures of the control specimen and specimens containing 10% and 20% metakaolin have been discussed in the above section. The corresponding XRD re-

sults are shown in Figure 6. The phase evolution of the specimens can be recognized by identifying the peak positions. The major phases are  $\text{Ca(OH)}_2$ , ettringite (AFt) and tricalcium silicate ( $\text{C}_3\text{S}$ ). Due to the pozzolanic reaction of metakaolin, the evolution of calcium hydroxide is the main phase which is identified. From Figure 6, it can be noticed that the intensity of  $\text{Ca(OH)}_2$  is lower in the specimen containing metakaolin compared to the control specimen. In addition, the intensity of  $\text{Ca(OH)}_2$  decreases gradually as the metakaolin increases. The XRD results reveal that  $\text{Ca(OH)}_2$  can be consumed by the addition of metakaolin.

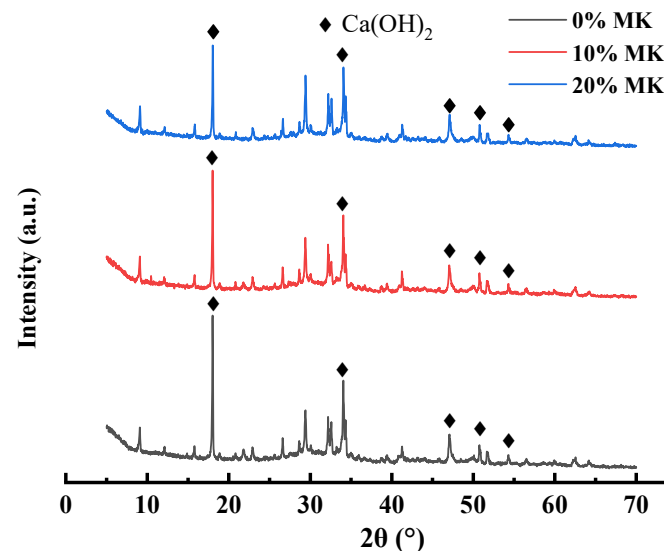


**Figure 6.** The microstructure of concrete at 0.45  $w/c$  ratio at 28 days.

### 3.8. Comparison between Experimental Results and Predictions by Design Code Expressions and Empirical Models

It is well-known that there is an inherent relationship between the compressive strength and the elastic modulus, the ultrasonic pulse velocity and the rebound number. Several design code expressions and empirical models have been proposed to predict the physical and mechanical properties of concrete. In terms of the relationship between elasticity modulus and compressive strength, a series of specifications have been established for prediction, as listed in Table 4. Figure 7 shows the experiment results and the predicted results by design code expressions. It can be observed that the experimental results are quite close to the predicted values by ACI-318, JSCE-07, CSA A23.3-04, JCI-08, EC-09 and NZS 3101 [51–54]. However, it can be noticed that the predicted results of EC-04 and JCI-08 are remarkably higher than the experimental results. In addition, there are no existing design code expressions in the relationship between compressive strength, ultrasonic pulse velocity and the rebound number. However, as reported by Muduli, there is a linear relationship between compressive strength, ultrasonic pulse velocity and rebound number [6]. The linear fitting results are shown in Figures 8 and 9. It can be found that the correlation coefficient ( $R^2$ ) is 0.98 and 0.92 for compressive strength, ultrasonic wave velocity and rebound number. As expected, the fitting results are favorable.

**Table 4.** The design code expressions and empirical models for estimating the elastic modulus based on the compressive strength.

Design Code	Elastic Modulus (GPa)	Design Code	Elastic Modulus (GPa)
ACI-318	$E_c = 4.73\sqrt{f_c}$	JCI-08	$E_c = 6.3f_c^{0.45}$
JSCE-07	$E_c = 4.7\sqrt{f_c}$	EC-04	$E_c = 22(f_c/10)^{0.3}$
CSA A23.3-04	$E_c = 4.5\sqrt{f_c}$	NZS 3101	$E_c = 3.32(\sqrt{f_c}) + 6.9$

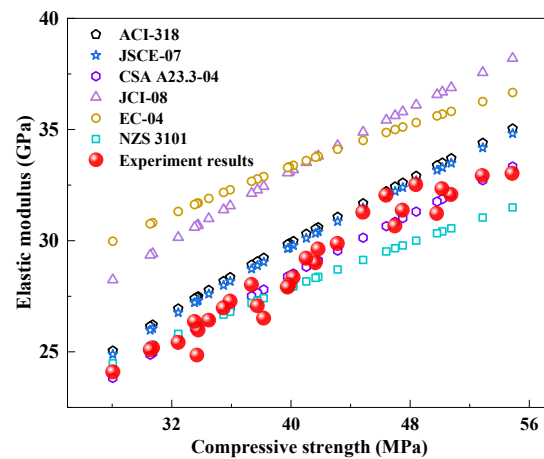


Figure 7. The relationship between the elasticity modulus and compressive strength.

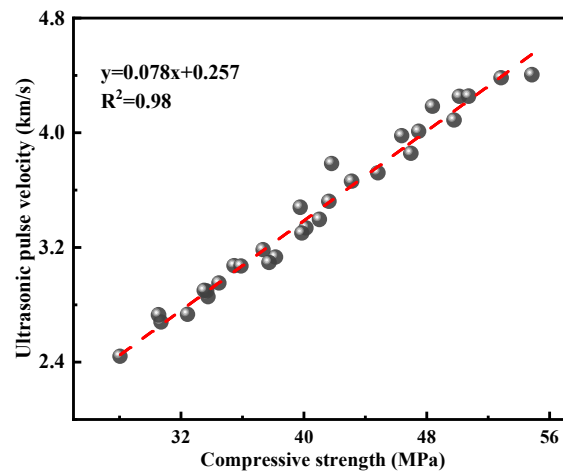


Figure 8. The relationship between the ultrasonic pulse velocity and compressive strength.

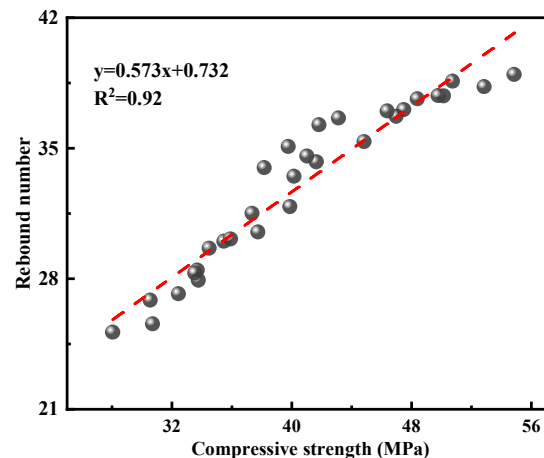


Figure 9. The relationship between the rebound number and compressive strength.

#### 4. Predicting Concrete Strength by ELM

##### 4.1. Establishment of ELM

ELM is an improved analytical method based on a traditional artificial neural network (ANN). ELM has two representative advantages: (1) The connection weights and thresholds of the hidden layer can be randomly set; (2) there is no iterative adjustment in connection weights between the hidden layer and the output layer. Due to the above reasons, ELM can

save a great deal of calculation time compared with ANN. In addition, ELM has achieved favorable performance in its ease of use, its high generalization ability and its precision. In this paper, the most basic extreme learning machine is selected, and the nuclear extreme learning machine is not used. The activation function is sigmoidal. At the same time, since the population optimization algorithm based on biology is not adopted, the optimization of the extreme learning machine is not involved, so the optimal working condition is not involved.

ELM is an algorithm proposed as SLFNs. Its general structure is shown in Figure 10. The prediction method was completed by using MATLAB R2018a and Excel 2016, and illustrations were made by using software such as Origin 2019b, ArcMap 10.7 and Visio 2016. When modeling data using an ELM model, the following simple four-step process is used: (1) randomly produce hidden layer weights and biases (rather than iteratively construct like the ANN model); (2) generate a hidden layer output matrix using the produced hidden layer parameters; (3) calculate the output weights by inverting the hidden layer output matrix using the Moore–Penrose generalized inverse matrix; and (4) calculate the product of the matrix using the response variable.

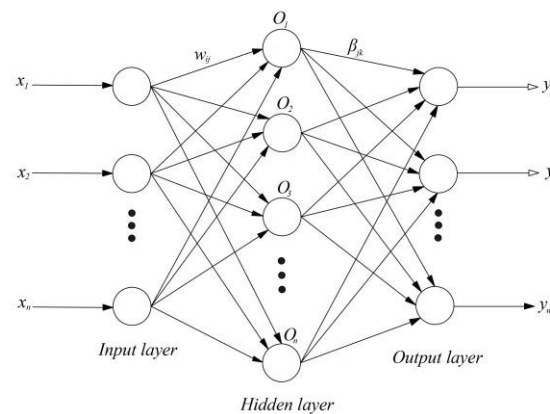


Figure 10. General structure diagram.

The principle of ELM is as follows:

It is supposed that there are  $N$  arbitrary samples  $X_j = [x_{j1}, x_{j2}, \dots, x_{jn}]^T \in R^n, j = 1, \dots, N$ ;  $Y_j = [y_{j1}, y_{j2}, \dots, y_{jm}]^T \in R^m, j = 1, \dots, N$ . For a single hidden layer of feed forward networks with  $L$  hidden nodes with activation function  $g(x)$ , the mathematical equation can be written as follows [54]:

$$\sum_{i=1}^L \beta_i g(W_i \cdot X_j + b_i) = O_j, j = 1, \dots, N \tag{1}$$

where  $W_i$  denotes the weight matrix between the input and hidden nodes,  $\beta_i$  denotes the weight matrix between the hidden neurons and the output neurons,  $b_i$  denotes the bias of the hidden layer and  $W_i \cdot X_j$  represents inner product of  $W$  and  $X_j$  [55].

The goal of learning is to minimize the error of output, which can be expressed as:

$$\sum_{j=1}^N \|O_j - y_j\| = 0 \tag{2}$$

In other words, there is a relationship as follows:

$$\sum_{i=1}^L \beta_i g(W_i \cdot X_j + b_i) = y_j, j = 1, \dots, N \tag{3}$$

It can be expressed as a matrix, as follows:

$$H\beta = Y; \tag{4}$$

$$H(W_1, \dots, W_L, b_1, \dots, b_L, X_1, \dots, X_L) = \begin{bmatrix} g(W_1 \cdot X_1 + b_1) & \dots & g(W_L \cdot X_1 + b_L) \\ \vdots & \ddots & \vdots \\ g(W_1 \cdot X_N + b_1) & \dots & g(W_L \cdot X_N + b_L) \end{bmatrix}_{N \times L}; \tag{5}$$

$$\beta = \begin{bmatrix} \beta_1^T \\ \vdots \\ \beta_L^T \end{bmatrix}_{L \times m}; Y = \begin{bmatrix} Y_1^T \\ \vdots \\ Y_N^T \end{bmatrix}_{N \times m} \tag{6}$$

where  $H$  is the output of the hidden node,  $T$  is the expected output and  $\beta$  is the output weight. According to orthogonal projection method and ridge regression theory, the  $\beta$  can be calculated as follows [56]:

$$\beta = (H^T H + \frac{I}{C})^{-1} H^T H \tag{7}$$

where  $C$  is the regularization coefficient, and  $I$  is the identity matrix. The coefficient of determination ( $R^2$ ), mean absolute error (MAE) and mean relative error (MAPE) are used to evaluate the performance of the model. These metrics are defined as follows:

$$R^2 = \frac{\sum_{i=1}^n (\hat{y}_i - \bar{y})^2}{\sum_{i=1}^n (y_i - \bar{y})^2} \tag{8}$$

$$MAE = \frac{1}{n} \sum_{i=1}^n |\hat{y}_i - y_i| \tag{9}$$

$$MAPE = \frac{1}{n} \sum_{i=1}^n \left| \frac{\hat{y}_i - y_i}{y_i} \right| \times 100\% \tag{10}$$

where  $n$  is the number of test samples,  $\hat{y}_i$  and  $y_i$  are the predicted and actual values of water quality at time  $i$  and  $\bar{y}$  is the mean value of the actual values. Among them, MAE and MAPE are three common error evaluation indicators, and the smaller their values, the smaller the error. The larger the value of  $R^2$ , the better the prediction quality. The results are shown in Table 5.

**Table 5.** Summary of error statistics of applied models.

Station	$R^2$	MAE	MAPE
Training set	0.99	0.99	5.71
test set	0.98	1.69	9.09

#### 4.2. Analysis of Training and Testing

The compressive strength of concrete depends on the mixing design and curing age. In other words, there is a complex nonlinear relationship between the mixing scheme, the curing regime and the compressive strength. In this section, ELM is applied to the predicted compressive strengths in scenarios with different mixing designs and curing ages. Age, water, cement, metakaolin, sand, coarse aggregate and CG served as the input parameters of ELM. The compressive strength is regarded as the output. The corresponding data can be found in Table 2 and Figure 1. A total of 90 sets of data were fed into the ELM, with 75 sets for training and the rest for prediction. The statistical characteristics of the data used are shown in Table 6. The predicting results of training and testing are plotted in Figure 11. It can be observed that the  $R^2$  obtained by training and testing are 0.99 and 0.98, respectively. This implies that the predicted compressive strength of concrete is comparable to the experimental results. The error of machine learning is within 10%, while the error of the design code expressions and empirical models is more than 10%. The prediction results obtained by extreme learning machines have superior performance compared to the design

code expressions and empirical models. From the above discussion, it is obvious that ELM can establish the complex nonlinear relationship between inputs (the mixture and curing age) and output (compressive strength). This also suggests that ELM is feasible to predict compressive strength of concrete containing CG and metakaolin.

**Table 6.** Statistical characteristics of the data used.

Station	Range	Average	Standard Deviation	Coefficient of Variation
Training set	7.60–51.57	24.25	124.69	5.14
test set	8.18–55.77	27.43	183.61	6.69

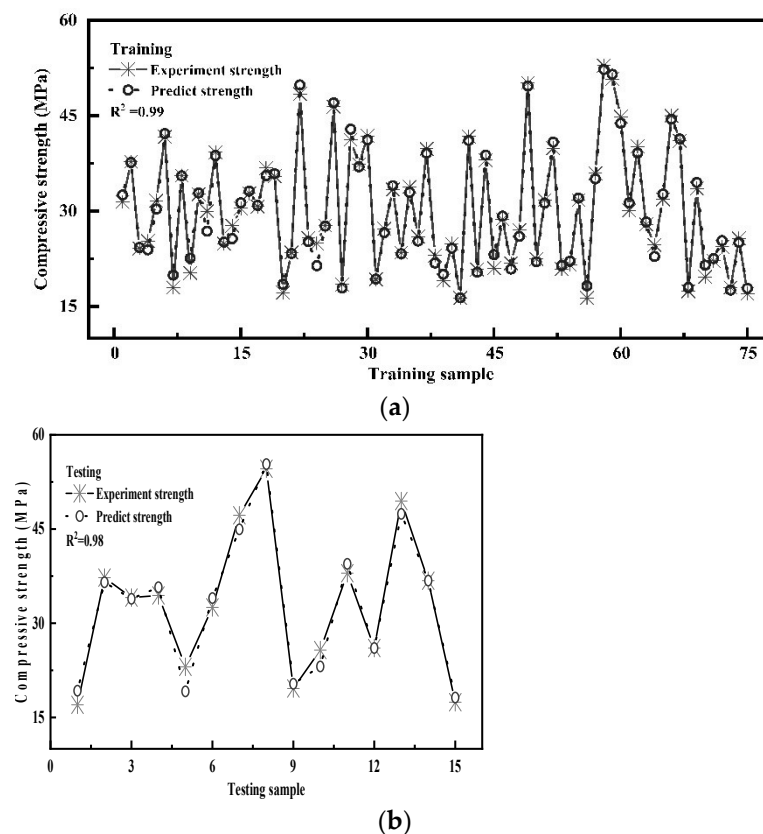


**Figure 11.** The results of training and testing. (a) Training sample; (b) Testing sample.

## 5. Conclusions

In this research, metakaolin and CG, as solid wastes, were applied to produce backfill concrete. Several experiments have been conducted to investigate the physical and mechanical properties of concrete containing metakaolin and CG. In addition, the relationships between compressive strength and elasticity modulus, ultrasonic pulse velocity as well as rebound number were revealed by design code expressions and empirical models. Furthermore, ELM, as an analytical model, was proposed to estimate compressive strength of concrete. The following conclusions can be drawn from this work:

- The compressive strength of concrete directly related to replacement level of metakaolin and CG. The inclusion of CG in concrete results in strength degradation, especially at a replacement level higher than 50%. However, this degradation can be remedied by the incorporation of metakaolin.
- The incorporation of <20% metakaolin and <50% CG in the specimens showed a higher or equivalent 28-day compressive strength compared with that of the control specimen. From the point of view of the environment and the economy, the replacement level of metakaolin and CG can be further increased. Compared to the control specimen,

the specimen with 20% metakaolin and 75% of CG showed less than a 5% decline in compressive strength, which is acceptable.

- The inclusion of CG in concrete results in low deformation resistance and high dispersion. These drawbacks can be mitigated by the incorporation of metakaolin.
- ANN, as a feasible and reliable method, is developed to predict compressive strength with high accuracy. Age, water, cement, metakaolin, sand, coarse aggregate and CG emerged as reliable predictors of compressive strength of concrete by ELM.

**Author Contributions:** Conceptualization, J.J.; data curation, S.Y.; formal analysis, Z.L.; funding acquisition, J.J.; investigation, Z.L.; methodology, S.Y.; project administration, J.J.; resources, J.J.; software, S.Y.; supervision, S.Y.; validation, Q.S.; visualization, Q.S.; writing—original draft, J.J.; writing—review and editing, Z.L. All authors have read and agreed to the published version of the manuscript.

**Funding:** This research was substantially funded by the National Natural Science Foundation of China (51974145, 51904144), Scientific research fund project of Education Department of Liaoning Province (LJKZ0354) and Project supported by the Discipline Innovation Team of Liaoning Technical University (Key Laboratory of Sichuan Province for Comprehensive Development and Utilization of Civil Engineering of Industrial Solid Waste) (SC\_FQWLY-2020-Y-01).

**Data Availability Statement:** All data supporting the findings in this study are available from the corresponding author on reasonable request.

**Acknowledgments:** This research was financially supported by the National Natural Science Foundation of China (grant numbers 51974145, 51904144) and the Scientific research fund project of the Education Department of Liaoning Province (grant number LJKZ0354) and Project supported by Discipline Innovation Team of Liaoning Technical University (Key Laboratory of Sichuan Province for Comprehensive Development and Utilization of Civil Engineering of Industrial Solid Waste) (grant numbers SC\_FQWLY-2020-Y-01).

**Conflicts of Interest:** The authors declare that they have no known competing financial interests or personal relationships that could have appeared to influence the work reported in this paper.

## References

1. Dang, V.Q.; Ogawa, Y.; Bui, P.T.; Kawai, K. Effects of chloride ions on the durability and mechanical properties of sea sand concrete incorporating supplementary cementitious materials under an accelerated carbonation condition. *Constr. Build. Mater.* **2016**, *274*, 122016. [[CrossRef](#)]
2. Liu, C.; Deng, X.; Liu, J.; Hui, D. Mechanical properties and microstructures of hypergolic and calcined coal gangue based geopolymer recycled concrete. *Constr. Build. Mater.* **2019**, *211*, 691–708. [[CrossRef](#)]
3. Yuan, Y.; Shao, Z.; Qiao, R.; Fei, X.; Cheng, J.; Wei, W. Fracture behavior of concrete coarse aggregates under microwave irradiation influenced by mineral components. *Constr. Build. Mater.* **2021**, *286*, 122944. [[CrossRef](#)]
4. Li, Y.; Liu, S.; Guan, X. Multitechnique investigation of concrete with coal gangue. *Constr. Build. Mater.* **2021**, *301*, 124114. [[CrossRef](#)]
5. Bari, H.; Salama, M.A.; Safiuddin, M. Fresh and hardened properties of brick aggregate concrete including coconut shell as a partial replacement of coarse aggregate. *Constr. Build. Mater.* **2021**, *297*, 123745. [[CrossRef](#)]
6. Muduli, R.; Mukharjee, B.B. Effect of incorporation of metakaolin and recycled coarse aggregate on properties of concrete. *J. Clean. Prod.* **2019**, *209*, 398–414. [[CrossRef](#)]
7. Huang, G.; Ji, Y.; Li, J.; Hou, Z.; Dong, Z. Improving strength of calcinated coal gangue geopolymer mortars via increasing calcium content. *Constr. Build. Mater.* **2018**, *166*, 760–768. [[CrossRef](#)]
8. Sharifi, Y.; Adshoon, I.; Asad-Abadi, S.; Aslani, F. Environmental protection by using waste copper slag as a coarse aggregate in self-compacting concrete. *J. Environ. Manag.* **2020**, *271*, 111013. [[CrossRef](#)]
9. Li, P.P.; Cao, Y.Y.; Sluijsmans, M.J.C.; Brouwers, H.J.H.; Yu, Q. Synergistic effect of steel fibres and coarse aggregates on impact properties of ultra-high performance fibre reinforced concrete. *Cem. Concr. Compos.* **2021**, *115*, 103866. [[CrossRef](#)]
10. Karimipour, A. Effect of untreated coal waste as fine and coarse aggregates replacement on the properties of steel and polypropylene fibres reinforced concrete. *Mech. Mater.* **2020**, *150*, 103592. [[CrossRef](#)]
11. Guan, X.; Chen, J.; Qiu, J.; Gao, Y.; Gao, J. Damage evaluation method based on ultrasound technique for gangue concrete under freezing-thawing cycles. *Constr. Build. Mater.* **2020**, *246*, 118437. [[CrossRef](#)]
12. Park, I.; Tabelin, C.B.; Jeon, S.; Li, X.; Seno, K.; Ito, M.; Hiroyoshi, N. A review of recent strategies for acid mine drainage prevention and mine tailings recycling. *Chemosphere* **2019**, *219*, 588–606. [[CrossRef](#)] [[PubMed](#)]

13. Tabelin, C.B.; Park, I.; Phengsaart, T.; Jeon, S.; Villacorte-Tabelin, M.; Alonzo, D.; Yoo, K.; Ito, M.; Hiroyoshi, N. Copper and critical metals production from porphyry ores and E-wastes: A review of resource availability, processing/recycling challenges, socio-environmental aspects, and sustainability issues. *Resour. Conserv. Recycl.* **2021**, *170*, 105610. [[CrossRef](#)]
14. Tabelin, C.B.; Dallas, J.; Casanova, S.; Pelech, T.; Bournival, G.; Saydam, S.; Canbulat, I. Towards a low-carbon society: A review of lithium resource availability, challenges and innovations in mining, extraction and recycling, and future perspectives. *Miner. Eng.* **2021**, *163*, 106743. [[CrossRef](#)]
15. Huyen, D.T.; Tabelin, C.B.; Thuan, H.M. The solid-phase partitioning of arsenic in unconsolidated sediments of the Mekong Delta, Vietnam and its modes of release under various conditions. *Chemosphere* **2019**, *233*, 512–523. [[CrossRef](#)]
16. Tabelin, C.B.; Igarashi, T.; Villacorte-Tabelin, M.; Park, I.; Opiso, E.M.; Ito, M.; Hiroyoshi, N. Arsenic, selenium, boron, lead, cadmium, copper, and zinc in naturally contaminated rocks: A review of their sources, modes of enrichment, mechanisms of release, and mitigation strategies. *Sci. Total Environ.* **2018**, *645*, 1522–1553. [[CrossRef](#)]
17. Arima, T.; Sasaki, R.; Yamamoto, T.; Tabelin, C.B.; Tamoto, S.; Igarashi, T. Effects of environmental factors on the leaching and immobilization behavior of arsenic from mudstone by laboratory and in situ column experiments. *Minerals* **2021**, *11*, 1220. [[CrossRef](#)]
18. Li, J.M.; Huang, Y.L.; Ouyang, S.; Guo, Y.; Gao, H.; Wu, L.; Shi, Y.; Zhu, L. Transparent characterization and quantitative analysis of broken gangue's 3D fabric under the bearing compression. *Int. J. Min. Sci. Technol.* **2021**, *11*, 13. [[CrossRef](#)]
19. Li, J.M.; Huang, Y.L.; Li, W.; Guo, Y.; Ouyang, S.; Cao, G. Study on dynamic adsorption characteristics of broken coal gangue to heavy metal ions under leaching condition and its cleaner mechanism to mine water. *J. Clean. Prod.* **2021**, *329*, 1–12. [[CrossRef](#)]
20. Qiu, J.; Zhu, M.; Zhou, Y.; Guan, X. Effect and mechanism of coal gangue concrete modification by fly ash. *Constr. Build. Mater.* **2021**, *294*, 123563. [[CrossRef](#)]
21. Zhou, M.; Dou, Y.; Zhang, Y.; Zhang, Y.; Zhang, B. Effects of the variety and content of coal gangue coarse aggregate on the mechanical properties of concrete. *Constr. Build. Mater.* **2019**, *220*, 386–395. [[CrossRef](#)]
22. Wang, Q.; Li, Z.; Zhang, Y.; Zhang, H.; Zhou, M.; Fang, Y. Influence of coarse coal gangue aggregates on elastic modulus and drying shrinkage behaviour of concrete. *J. Build. Eng.* **2020**, *32*, 101748. [[CrossRef](#)]
23. Juenger, M.C.G.; Siddique, R. Recent advances in understanding the role of supplementary cementitious materials in concrete. *Cem. Concr. Res.* **2015**, *78*, 71–80. [[CrossRef](#)]
24. John, V.M.; Damineli, B.L.; Quattrone, M.; Pileggi, R.G. Fillers in cementitious materials—Experience, recent advances and future potential. *Cem. Concr. Res.* **2018**, *114*, 65–78. [[CrossRef](#)]
25. Monteiro, P.J.M.; Geng, G.; Marchona, D.J.; Li, J.; Alapati, P.; Kurtis, K.E.; Qomi, M.J.A. Advances in characterizing and understanding the microstructure of cementitious materials. *Cem. Concr. Res.* **2019**, *124*, 105806. [[CrossRef](#)]
26. Skibsted, J.; Snellings, R. Reactivity of supplementary cementitious materials (SCMs) in cement blends. *Cem. Concr. Res.* **2019**, *124*, 105799. [[CrossRef](#)]
27. Karahan, O.; Hossain, K.M.A.; Ozbay, E.; Lachemi, M.; Sancak, E. Effect of metakaolin content on the properties self-consolidating lightweight concrete. *Constr. Build. Mater.* **2012**, *31*, 320–325. [[CrossRef](#)]
28. Salimi, J.; Ramezani-pour, A.M.M.; Moradi, J. Studying the effect of low reactivity metakaolin on free and restrained shrinkage of high performance concrete. *J. Build. Eng.* **2020**, *28*, 101053. [[CrossRef](#)]
29. Güneş, E.; Gesoglu, M.; Karaoglu, S.; Mermerdas, K. Strength permeability and shrinkage cracking of silica fume and metakaolin concretes. *Constr. Build. Mater.* **2012**, *34*, 120–130. [[CrossRef](#)]
30. Dabbaghi, F.; Sadeghi-Nik, A.; Libre, N.A.; Nasrollahpour, S. Characterizing fiber reinforced concrete incorporating zeolite and metakaolin as natural pozzolans. *Structures* **2021**, *34*, 2617–2627. [[CrossRef](#)]
31. Sujjavanich, S.; Suwanvitaya, P.; Chaysuwan, D.; Heness, G. Synergistic effect of metakaolin and fly ash on properties of concrete. *Constr. Build. Mater.* **2017**, *155*, 830–837. [[CrossRef](#)]
32. Hasnaoui, A.; Ghorbel, E.; Wardeh, G. Performance of metakaolin/slag-based geopolymer concrete made with recycled fine and coarse aggregates. *J. Build. Eng.* **2021**, *42*, 102813. [[CrossRef](#)]
33. Xie, J.; Zhang, H.; Duan, L.; Yang, Y.; Yan, J.; Shan, D.; Liu, X.; Pang, J.; Chen, Y.; Li, X.; et al. Effect of nano metakaolin on compressive strength of recycled concrete. *Constr. Build. Mater.* **2020**, *256*, 119393. [[CrossRef](#)]
34. Singh, N.; Mithulraj, M.; Arya, S. Utilization of coal bottom ash in recycled concrete aggregates based self-compacting concrete blended with metakaolin. *Resour. Conserv. Recycl.* **2019**, *144*, 240–251. [[CrossRef](#)]
35. GB175–2007; Common Portland Cement. Chinese Standard: Beijing, China, 2007.
36. Jin, J.; Qin, Z.; Lü, X.; Liu, T.; Zhang, G.; Shi, J.; Zuo, S.; Li, D. Rheology control of self-consolidating cement-tailings grout for the feasible use in coal gangue-filled backfill. *Constr. Build. Mater.* **2022**, *316*, 125836. [[CrossRef](#)]
37. Silwamba, M.; Ito, M.; Hiroyoshi, N.; Tabelin, C.B.; Fukushima, T.; Park, I.; Jeon, S.; Igarashi, T.; Sato, T.; Nyambe, I.; et al. Detoxification of lead-bearing zinc plant leach residues from Kabwe, Zambia by coupled extraction-cementation method. *J. Environ. Chem. Eng.* **2020**, *8*, 104197. [[CrossRef](#)]
38. Tabelin, C.B.; Silwamba, M.; Paglinawan, F.C.; Mondejar, A.J.S.; Duc, H.G.; Resabal, V.J.; Opiso, E.M.; Igarashi, T.; Tomiyama, S.; Ito, M.; et al. Solid-phase partitioning and release-retention mechanisms of copper, lead, zinc and arsenic in soils impacted by artisanal and small-scale gold mining (ASGM) activities. *Chemosphere* **2020**, *260*, 127574. [[CrossRef](#)]
39. GB/T 50081-2019; Standard for Test Method of Mechanical Properties on Ordinary Concrete. Chinese Standard: Beijing, China, 2019.

40. CECS 21:2000; Technical Specification for Inspection of Concrete Defects by Ultrasonic Method. Chinese Standard: Beijing, China, 2000.
41. JGJ/T 23-2011; Technical Specification for Inspection of Concrete Defects by Rebound Method. Chinese Standard: Beijing, China, 2011.
42. ASTM C642-13; Standard Test Method for Density, Absorption, and Voids in Hardened Concrete. American Society for Testing and Materials: West Conshohocken, PA, USA, 2013.
43. Li, X.L.; Gao, M.; Hiroyoshi, N.; Tabelin, C.B.; Taketsugu, T.; Ito, M. Suppression of pyrite oxidation by ferric-catecholate complexes: An electrochemical study. *Miner. Eng.* **2019**, *138*, 226–237. [[CrossRef](#)]
44. Park, I.; Tabelin, C.B.; Seno, K.; Jeon, S.; Inano, H.; Ito, M.; Hiroyoshi, N. Carrier-microencapsulation of arsenopyrite using Al-catecholate complex: Nature of oxidation products, effects on anodic and cathodic reactions, and coating stability under simulated weathering conditions. *Heliyon* **2020**, *6*, e03189. [[CrossRef](#)]
45. Hua, X.; Shi, C.; Shi, Z.; Zhang, L. Compressive strength, pore structure and chloride transport properties of alkali-activated slag/fly ash mortars. *Cem. Concr. Compos.* **2019**, *104*, 103392. [[CrossRef](#)]
46. Aseniero, J.P.J.; Opiso, E.M.; Banda, M.H.T.; Tabelin, C.B. Potential utilization of artisanal gold-mine tailings as geopolymeric source material: Preliminary investigation. *SN Appl. Sci.* **2019**, *1*, 35. [[CrossRef](#)]
47. Opiso, E.M.; Tabelin, C.B.; Maestre, C.V.; Aseniero, I.P.J.; Park, I.; Villacorte-Tabelin, M. Synthesis and characterization of coal fly ash and palm oil fuel ash modified artisanal and small-scale gold mine (ASGM) tailings based geopolymer using sugar mill lime sludge as Ca-based activator. *Heliyon* **2021**, *7*, e06654. [[CrossRef](#)] [[PubMed](#)]
48. Li, Q.; Geng, H.; Shui, Z.; Huang, Y. Effect of metakaolin addition and seawater mixing on the properties and hydration of concrete. *Appl. Clay Sci.* **2015**, *115*, 51–60. [[CrossRef](#)]
49. Dadsetan, S.; Bai, J. Mechanical and microstructural properties of self-compacting concrete blended with metakaolin, ground granulated blast-furnace slag and fly ash. *Constr. Build. Mater.* **2017**, *146*, 658–667. [[CrossRef](#)]
50. Sharma, R.; Khan, R.A. Influence of copper slag and metakaolin on the durability of self-compacting concrete. *J. Clean. Prod.* **2018**, *171*, 1171–1186. [[CrossRef](#)]
51. ACI 318-11, ACI Committee; American Concrete Institute; International Organization for Standardization. *Building Code Requirements for Structural Concrete and Commentary*; American Concrete Institute: Farmington Hills, MI, USA, 2011.
52. Japan Society of Civil Engineers, JSCE No. 15. *Standard Specification for Concrete Structure*; Japanese Society of Civil Engineering: Tokyo, Japan, 2007.
53. CSA. *Design of Concrete Structures*; Canadian Standard Association: Mississauga, ON, Canada, 2004.
54. Xue, Y.; Bai, C.; Qiu, D.; Kong, F.; Li, Z. Predicting rock burst with database using particle swarm optimization and extreme learning machine. *Tunn. Undergr. Space Technol.* **2020**, *98*, 1–12. [[CrossRef](#)]
55. Al-Shamiri, A.K.; Kim, J.H.; Yuan, T.F.; Yoon, Y.S. Modeling the compressive strength of high-strength concrete: An extreme learning approach. *Constr. Build. Mater.* **2019**, *208*, 204–219. [[CrossRef](#)]
56. Su, X.; An, J.; Zhang, Y.; Zhu, P.; Zhu, B. Prediction of ozone hourly concentrations by support vector machine and kernel extreme learning machine using wavelet transformation and partial least squares methods. *Atmos. Pollut. Res.* **2020**, *11*, 024. [[CrossRef](#)]